Madariaga, A., Perez, I., Arrazola, P.J. *et al.* Reduction of distortions in large aluminium parts by controlling machining-induced residual stresses. *Int J Adv Manuf Technol* **97**, 967–978 (2018). https://doi.org/10.1007/s00170-018-1965-2

Reduction of distortions in large aluminium parts by controlling machining-induced residual stresses

A. Madariaga *(1), I. Perez (1), P.J. Arrazola (1), R. Sanchez (2), J.J. Ruiz (2), F.J. Rubio (2)

[1] Mechanical and Industrial Production Department, Faculty of Engineering, Mondragon Unibertsitatea, Spain

[2] Aerometallic (Aernnova Group), Spain

Corresponding author:

Aitor Madariaga, Mechanical and Industrial Production Department, Faculty of Engineering, Mondragon Unibertsitatea, Loramendi 4, 20500 Mondragon, Spain.

E-mail address: amadariaga@mondragon.edu

Abstract

Large aluminium monolithic parts used in the aeronautic industry frequently show significant geometric distortions after the machining process. These distortions are the consequence of the initial residual stresses of the raw material as well as machining-induced residual stresses. Therefore, to minimise distortions it is fundamental to understand the effect of the different parameters of the manufacturing process and define the optimum manufacturing strategy.

This work studies the effect of initial residual stresses of aluminium plates and the residual stresses generated by the machining process on the final geometric distortions of the part. First, 7175-T7351 aluminium bars (40 mm wide × 38 mm thick × 400 mm long) were face milled at two different cutting conditions reducing the thickness to 6 mm. The distortions were measured in a CMM machine. The results revealed that the machining strategy significantly influenced the distortions, as a difference of 65% on distortions was found between the two cutting conditions. In addition, an FEM model to predict distortions was developed. This model considers initial residual stresses (measured by the contour method) and residual stresses induced by the machining process (measured by the hole drilling technique). Once the FEM model was validated, the study was extended to more complex geometries. These new studies revealed that final distortions are sensitive to machining-induced residual stresses. Furthermore, this finding indicates that it is possible to define machining conditions which generate desirable residual stress profiles to minimise part distortion.

Keywords

Aerospace, Machining, Distortions, Residual Stress

1. Introduction

The demand for fuel-efficient and lightweight aircraft has promoted the use of high strength and damage tolerant alloys to enable the design of thinner web and wall features in aeronautical monolithic components [1]. Commonly, aluminium alloys are used to manufacture these monolithic parts due their high specific strength, low cost and good forming properties. Nevertheless, aeronautical aluminium alloy parts become easily distorted during the manufacturing process as a consequence of low stiffness of the large parts, higher inherent residual stresses, and high material removal rate up to 90% [2]. Final distortions require correction processes (i.e. peen forming) that increase the cost of the component or, in the worst-case scenario, lead to rejection of the part. A study conducted in Boeing regarding the information on manufacturing of four different aeroplanes, estimated that waste material and correcting processes of distortions generated in machined parts cost the company an additional 290BN USD [3]. Beyond this context, significant research studies have been carried out over the last 10 years to understand the main causes of distortions, and develop design and manufacturing processes that minimise the distortion problem.

Part distortion is defined as the form deviation of the final component shape with respect to the designed original part after being released from the clamping system [1]. Part distortion depends on the manufacturing process chain. In general, distortion in aluminium machined components is a consequence of the residual stresses in the bulk material (prior to the machining process) as well as machining-induced residual stresses [4]. The machining process removes the initial residual stresses in the material and induces new residual stresses in the machining affected surface layer [5]. Both effects

contribute to the final distortion of the machined component. Therefore, controlling the magnitude and distribution of the residual stresses is the main method to control the distortion of large aluminium parts [2].

One strategy to control the distribution of initial residual stresses is to modify the offset, which is defined as the position of the parts in the initial workpiece [6]. For instance, Cerutti [6] using FEM simulations found that an offset of 9.05 mm led to negligible distortions when machining a 68 mm thick aluminium part from an initial workpiece of 90 mm thickness. Although this approach can be quite useful to minimise part distortions, it generally requires initial workpieces much thicker than the final part, and consequently fly-to-buy ratio and manufacturing costs increase. With the cost consideration in mind, an interesting alternative to reduce part distortions is to control the residual stresses induced by the thermomechanical loads developed during the machining processes.

Denkena et al. [7] conducted a pioneering work to understand the influence of cutting conditions on part distortions of workpieces made of forged aluminium alloys. They side-milled two workpieces of Al 7449-T651 (400 × 400 × 76 mm initial dimensions) with different geometry under several cutting conditions. Importantly, they found that cutting speed does have a significant influence on part distortion; both workpiece geometries exhibited the lowest part distortions when machining at the highest cutting speed. Tang et al. [8] developed an FEM model to predict distortions in machined parts considering multifactor coupling effect including original residual stresses, cutting loads, clamping forces and machining residual stresses. The model provided deformation shapes and magnitudes close to experimental results in a 7050-T7451 aluminium part, however they analysed only one cutting condition. They explained that

the bending distortion was caused by original residual stresses, and machining residual stresses led to twist (due to shear stresses). Li et al. [9] studied the effect of depth of cut on the redistribution of residual stress and distortion during the milling of 2 mm thick flat plates of Al2024-T3 aluminium alloy. They found that obtaining the shallow layer profile of machining-induced residual stress and reducing the difference between the maximum surface and subsurface residual stress generates smaller machining distortions of thin-walled part. In a recent study, Masoudi et al. [3] analysed the effect of various machining conditions on residual stress distribution and their correlation with distortions when dry turning thin-walled cylinders made of Al7075-T6. They observed that with an increase in the machining-induced residual stresses and their depth, the imbalance in internal stress was increased, leading to more distortion.

Nevertheless, some other researchers have found that the effect of machining-induced residual stresses does not affect significantly part distortion. Yang and co-workers [10] studied experimentally and using FEM the effect of initial residual stresses and cutting loads (machining-induced residual stresses) on the distortions of a 7075 aluminium workpiece. They concluded that initial residual stresses are the main cause of distortion in aluminium monolithic parts, however they only analysed one machining condition. Huang et al. [11] studied experimentally and numerically the effects of material initial residual stresses and machining-induced residual stresses on the distortion of a 7050-T7451 aluminium monolithic beam. They found that initial residual stress was the main factor (accounted for 90% of the total distortion) and the influence of machining-induced residual stresses on final distortion was almost negligible (10%). However, it once again should be noted that only one machining condition was studied.

In general, for thick aluminium plates the effect of bulk residual stresses on the distortion of the machined part is the main factor. However, the influence of machining-induced residual stresses on the final distortion of thin-walled parts must be considered together with initial residual stresses. Unfortunatley, there have been no agreements about the critical value of material thickness, although some authors defined it as 3-4 mm [2].

The literature review concludes that the influence of machining-induced residual stresses on distortions of large aluminium parts is still unclear. Therefore, in order to reduce part distortions by controlling cutting conditions, it is necessary to gain understanding of the effect of machining-induced residual stresses on final part distortions.

This paper is aimed at understanding the effect of both initial residual stresses and machining-induced residual stresses on the final geometric distortions of aluminium parts. First, 7175-T7351 aluminium bars were face milled at two different cutting conditions, and the distortions were measured in a Coordinate Measuring Machine (CMM). An FEM model to predict distortions was developed. This model considers initial residual stresses (measured by the contour method) and residual stresses induced by the machining process (measured by the hole drilling technique). Once the FEM model was validated, the study was applied to a more complex geometry analysing the effect of machining-induced residual stresses of nine different combinations of cutting conditions. Based on these simulations, an analytical relationship was established between the machining-induced residual stresses and the distortion.

2. Materials and experiments

2.1. Material

Two different type of specimens were extracted by water jet assisted machining from a 38 mm thick aluminium 7175-T7351 plate. The specimens for the machining trials (Type I) were 380 mm long, 40 mm wide and 38 mm thick. The specimens (Type II) used to determine the initial residual stresses of the plate through the thickness were 100 mm long, 40 mm wide and 38 mm thick. The longitudinal direction of both type of specimens was aligned with the rolling direction of the plate as shown in Fig.1.

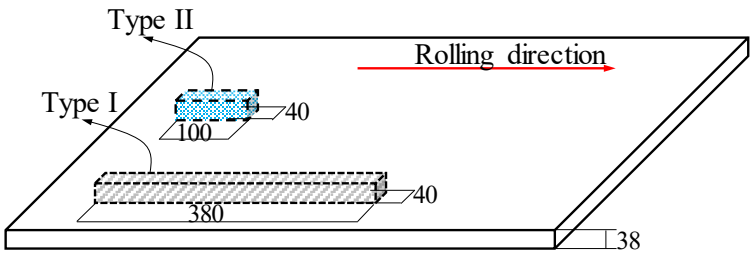

Fig. 1. Scheme of the specimens

2.2. Machining test and distortion measurements

The specimens Type I were face milled reducing the thickness to 6 mm, as can be seen in Fig. 2. Table 1 summarises the face milling conditions used in this work. All specimens were fixed to the table using wedge clamps (see Fig. 2), and they were face milled under identical roughing cutting conditions. Two different finishing cutting parameters were employed (finishing A and finishing B) to evaluate the effect of cutting conditions on machining-induced residual stresses and final distortions. The specimens were dry milled. An indexable face milling cutter with a diameter of 50 mm with five

uncoated inserts (APKT L93 1604PDFR) was used in the face milling tests. The properties of the inserts are shown in Table 2.

Table 1. Face milling conditions

Test	Cutting speed [m/min]	Feed [mm/tooth]	Depth of cut [mm]	Coolant
Roughing	275	0.15	1	No
Finishing A	275	0.15	0.25	No
Finishing B	550	0.15	0.5	No

Table 2. Properties of the APKT L93 1604PDFR tool

Material	Rake angle [°]	Clearance Angle [°]	Nose radius [mm]	Edge radius [μ m]
Uncoated WC-Co (Carbide)	11	8	0.2	12

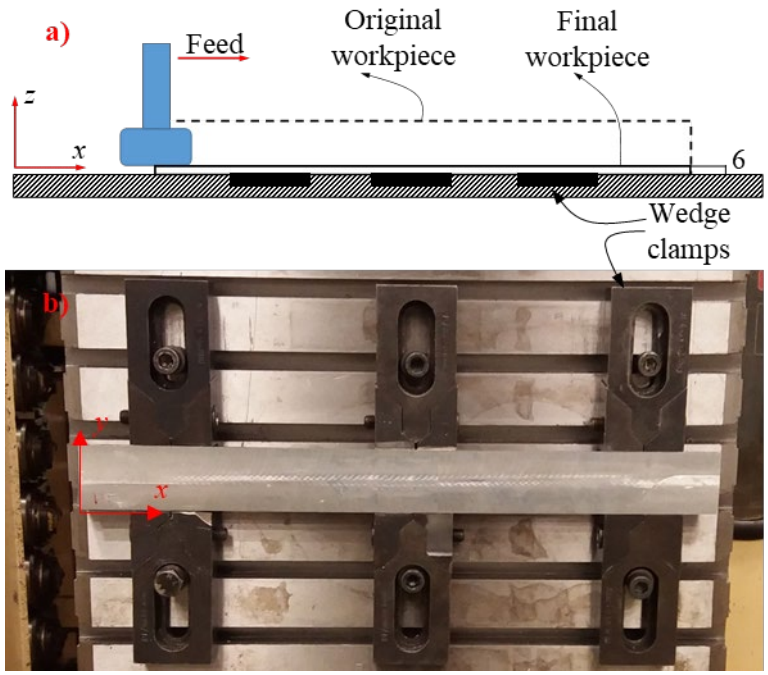

Fig. 2. a) Scheme of the face milling experiments and b) clamping system

After the face milling tests, the final distortions were measured in a CMM machine, Mitutoyo Crysta-Apex S 7106. As can be seen in Fig. 3, the vertical displacements (z direction) were measured along the longitudinal axis in the centre of the specimen.

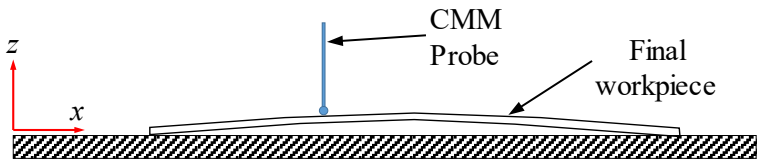

Fig. 3. Scheme of the CMM measurements

2.3. Measurement of initial residual stresses

As explained in the literature review, aluminium plates used in the manufacturing of aeronautic components possess initial residual stresses through the thickness, which contribute to the distortion of the machined part. In this work, the Contour Method developed by Prime [12] was used to measure the initial residual stresses in the longitudinal direction of the specimens. Specimens Type II described in the subsection 2.1 were used for that purpose.

Fig. 4 shows a scheme of the Contour Method procedure. First, the specimens were cut into two parts using the wire electric discharge machine. Due to the cut, the cross section of the resulting parts was deformed. The displacements perpendicular to the cross section (u_x) were measured in the CMM machine, using a spacing of 10 mm in the y direction (width) and 0.5 mm in the z direction (thickness). Then, the measured displacements were used to calculate the initial residual stresses in the longitudinal direction (perpendicular to the cut section) employing an elastic finite element analysis in the commercial software Abaqus Standard. The measured displacements were fitted

using fourth degree polynomial functions ($u_x = a \cdot z^4 + b \cdot z^3 + c \cdot z^2 + d \cdot z + e$; where a, b, c, d, e and f are the fitting parameters and z the coordinate along the thickness). Then, these displacements were applied as initial boundary conditions normal to the cut section in the finite element model but with opposite sign ($-u_x$). The model was meshed using C3D8 type hexahedral elements with 1 × 1 × 1 mm dimensions in the region close to the cut section. The opposite section was fixed to avoid rigid body motion. Finally, the linear elastic analysis determined the initial residual stresses normal to the cut section (σ_{xx}).

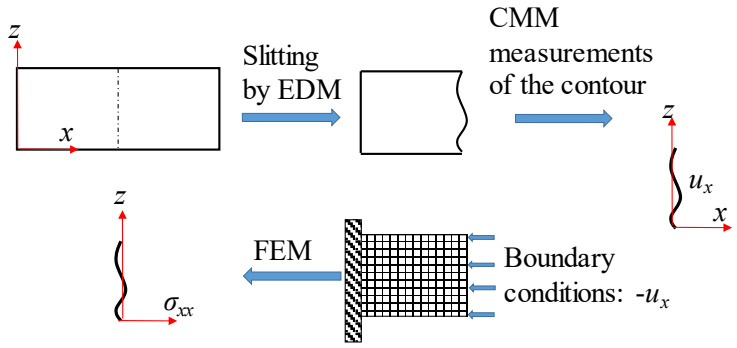

Fig. 4. Scheme of the Contour Method measurements

2.4. Machining-induced residual stress measurements

This research aims to study the effect of machining-induced residual stresses on part distortion. For that purpose, the machining-induced residual stresses were measured at the centre of the machined surfaces employing the hole drilling technique. The procedure given in the ASTM-E357 for hole drilling measurements was used. As residual stresses generated by machining processes are locked in a very shallow layer, the fine increment hole drilling procedure developed by Grant et al. [13] was followed.

The surfaces were prepared for gauge installation first by (a) applying a degreasing process using acetone, (b) wiping with 1000 grade abrasive paper (using light hand pressure), (c) following by the surface conditioning with water based acid surface cleaner and (d) neutralisation employing water based alkaline surface cleaner. After that Vishay Measurement Group target strain gauges EA-06-031RE-120 were bonded in the centreline (longest side) of the specimens. The tests were performed employing a Restan MTS3000 machine, using a high speed air turbine and drill bits of 0.8 mm diameter. The experimental set-up can be observed in Fig. 5. Before making the hole, the milling tool was aligned with the gauge. The zero depth was detected by electrical contact between the drill and the workpiece surface. Then, the incremental hole drilling procedure was carried out at each gauge employing a total of 15 depth increments. The first five increments had a depth of 10 µm, the next five increments had a depth of 20 µm, and the final five increments a depth of 50 µm. This sequence of increments produced a hole with a ≈0.9 mm diameter and a depth of 500 µm. Strains were recorded in a HBM data acquisition system after each increment. Finally, the residual stress profiles were calculated by the procedure given in the ASTM-E357.

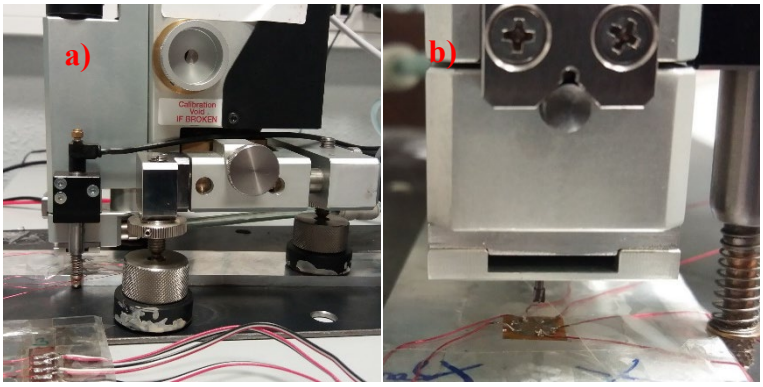

Fig. 5. a) Hole-drilling set-up for the machining-induced residual stress measurements and b) zoom of the drill bit

3. FEM Model

To predict the distortion of aluminium alloy aeronautical thin-walled parts two main different modelling strategies have been reported in the literature.

Some authors [14, 8] consider the effects of the physical process on the distortions of parts: the mechanical and thermal loads generated during cutting are applied to parts. The material removal is simulated to analyse the effect of the machining process, and in addition cutting forces and temperatures are introduced in the model when a volume of material is removed.

As summarized by Li et al. [2] in a recent literature review, an interesting modelling alternative to predict distortions of large aluminium parts consists of the superimposition of machining-induced residual stresses and bulk residual stresses. This modelling procedure does not simulate the cutting process but takes into account the final residual stress state of the machined part. In fact, machining-induced residual stresses are a consequence of the mechanical and thermal loads generated during the cutting process. For instance, this modelling procedure has been used satisfactorily by Jayanti et al. [15], and Denkena and Dreier [5] to predict distortions in thin-walled aluminium parts. In these models, the machining-induced residual stresses can be obtained experimentally, numerically or by means of an analytic model considering the cutting conditions as suggested by Wan et al.[16].

In order to study in detail the effect of both initial residual stresses and machining-induced residual stresses on the distortion of aluminium structural parts, an elastic finite element static model was employed. The model was used to simulate the two experimental tests described in subsection 2.2.

The model used in this study follows the simulation strategy developed by Denkena and Dreier [5]. For that purpose, the commercial Abaqus Standard software was used. Fig. 6 shows the lay-out of the FEM simulation procedure used to predict part distortions. It consists of three main steps: 1) introduction of initial residual stresses in the original workpiece, 2) removal of the material cut during the machining process and 3) adding machining-induced residual stresses in the machined surfaces. It should be noted that Fig. 6 only shows the stresses in *x* direction, although they have been introduced in both *x* and *y* directions.

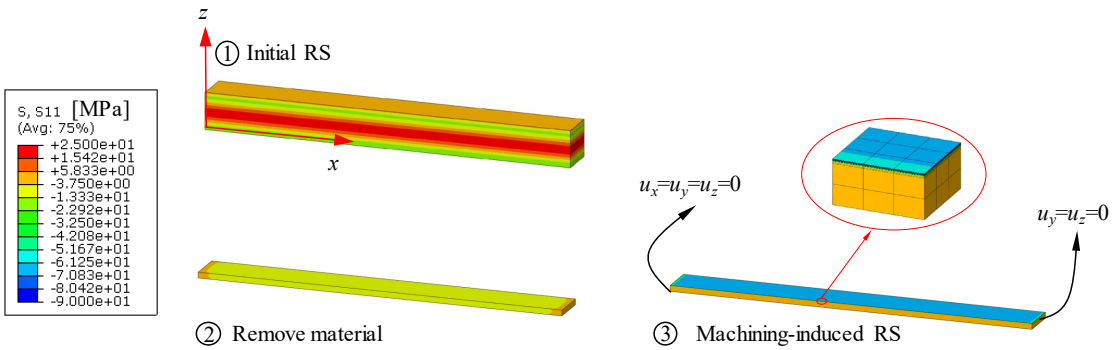

Fig. 6. Lay-out of the FEM model used to predict part distortion

The specimen Type I was used in the simulations, as it was used in the experiments. The Young's modulus of the 7175-T7351 aluminium was 71 GPa and the Poisson's ratio 0.33. The part was meshed using C3D8R type elements with a global nodal distance of 1 mm. As it will be explained later, the mesh was refined in the surface layer affected by the cutting process to add the machining-induced stresses. The measurements of the distortions depends on the boundary conditions. The distortion of simple geometries is mainly caused by bending (also evidenced in the experiments of this study). As can be seen in Fig. 6, the displacements of the left edge were restricted ($u_x=u_y=u_z=0$), and also the vertical and lateral displacements of the right edge ($u_y=u_z=0$).

These boundary conditions allowed predicting the curvature generated by bending distortions.

In the first step of the simulation the initial residual stresses of the original material were introduced throughout the workpiece, as shown in Fig. 6. These residual stresses were introduced employing the user-defined subroutine SIGINI in all active elements as function of coordinates. It was assumed that the distribution of the initial residual stresses was homogenous throughout the workpiece. The initial residual stresses were determined using the Contour Method as explained in the subsection 2.3 and the results can be seen in Fig. 7.

The second step of the simulation removes the material that it is cut in the machining experiments. In this model, all the elements contained in the layer from the top surface (z = 38 mm) to the final surface (z = 6 mm) were removed using the MODEL CHANGE, REMOVE interaction. This interaction allows deactivating and reactivating elements to simulate removal of part of the model, either temporarily or for the remainder of the analysis. As in the machining trials, the material removed by the roughing process was removed using layer with a thickness of 1 mm (depth of cut of the roughing process). In the cutting conditions named finishing A the last removed layer had a thickness of 0.25 mm and in the condition finishing B a thickness of 0.5 mm.

Finally, the machining-induced stresses are added in the third step as can be seen in Fig. 6. Machining-induced residual stresses are generated in very thin layers (usually thinner than 500 μm). Therefore, it is necessary to use a refined mesh near the machined surface. For that purpose, in this study the machining affected zone was divided into 7 thin layers. The five layers close to the surface had a thickness of 20 μm and the two

deepest layers a thickness of 50 μm, which gave a total thickness of 200 μm. As it was done in the experiments, two cutting conditions were simulated in this study. The residual stress profiles generated by the finishing A and finishing B conditions in the longitudinal direction (*x* direction) and transverse direction (*y* direction) of the specimen are shown in Fig. 8. It was assumed that the residual stress profile generated by the cutting process was homogenous in the machined surface.

4. Experimental results

4.1. Initial residual stresses

As explained in the introduction, the initial residual stresses locked in the material are removed during the machining process and affect the final part distortion. These residual stresses were measured using the Contour Method. Fig. 7 shows the longitudinal residual stress profiles throughout the thickness of the original material. The residual stress were compressive close to the upper and lower surfaces and tensile in the core region. The magnitude of the residual stresses was lower than 25 MPa, lower than 10% of the yield stress of the material ($\sigma_y \approx 435$ MPa). The aluminium plate used in this study was solution heat treated and specially aged to make the material resistant to stress-corrosion (heat treatment T7351). This heat treatment significantly reduced the residual stresses generated by the rolling process.

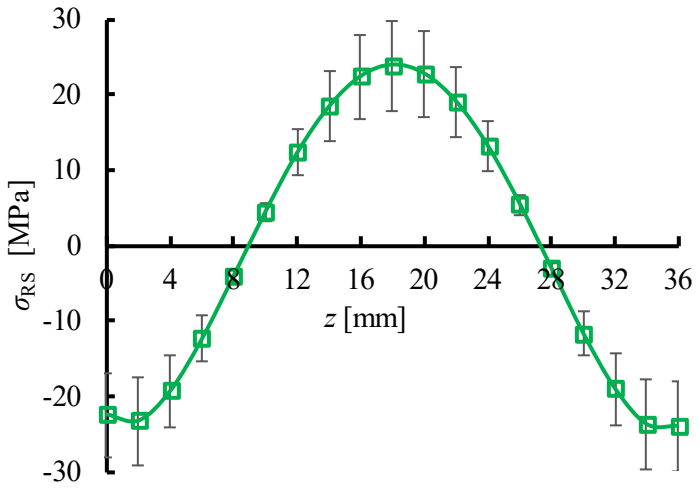

Fig. 7. Longitudinal residual stresses through the thickness of the original workpiece

4.2. Machining-induced residual stresses

The residual stress profiles generated by the face milling tests at the centre of the final surface of each specimen were measured employing the hole-drilling technique. Fig. 8 compares the average residual stress profiles in the longitudinal direction for finishing conditions A and B respectively. It is well known that machining-induced residual stresses are due to both, mechanical and thermal effects [17]. Plastic deformation induced by mechanical load generates compressive stresses in the surface layer and a thicker compressed layer. By contrast, plastic deformation induced by thermal load generates tensile stresses near the surface. The surface expands during heating whilst the subsurface does not. Then, on cooling, the surface tries to recover its position against the resistance of the subsurface, inducing tensile stresses at the surface. In this study, both testing conditions generated compressive residual stresses near the surface, which suggests that the thermal effect was not significant for the analysed cutting conditions. The maximum value of the compressive stress (110-130 MPa in the longitudinal direction and 110-160 in the transverse direction) was much lower than the

yield stress of the material. Finishing condition B, which used higher cutting speeds, and also higher depth of cut than condition A, generated higher compressive residual stress near the free surface in both directions. Nevertheless, finishing condition A induced a deeper compressive layer (≈150 µm) than condition B (≈100 µm).

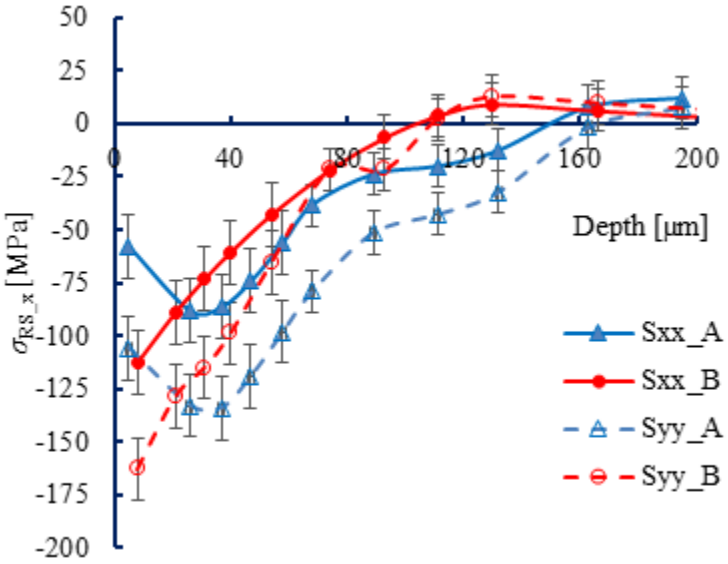

Fig. 8. Average longitudinal residual stresses generated by finishing conditions A and B

4.3. Experimental and simulated distortions

Fig. 9 compares the distortions (*z* displacement) of the specimens that were face milled under finishing condition A and finishing condition B respectively. Both machining conditions led to concave shape deformations of the specimens. The finishing condition B generated ≈0.15 mm maximum vertical displacement which was reached at the centre of the specimen. The finishing condition A caused 1.8-2.3 times higher maximum displacements than finishing condition B. These results confirm that cutting parameters have a significant influence on the distortion of thin-walled aluminium parts.

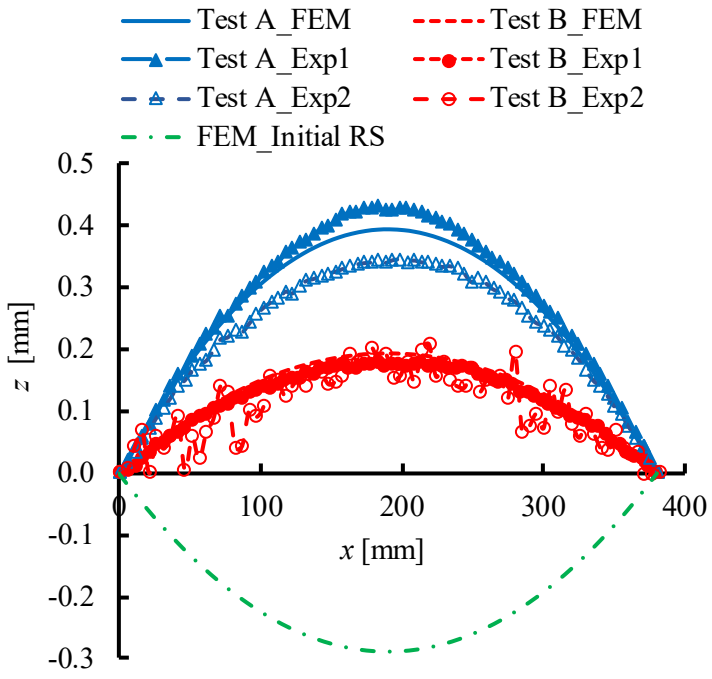

Fig. 9. Experimental and simulated vertical (z) displacements along the longitudinal direction (x)

The distortions simulated with the model described in section 3 are compared to experimental results in Fig. 9. The model predicted the distortions with an inaccuracy lower than 12% for both finishing conditions. An additional simulation was carried out considering only the effect of initial residual stresses of the original workpiece. This simulation produced a distortion of the specimen in the opposite direction. Therefore, the results confirm that machining-induced residual stresses significantly influence the final distortions.

5. Discussion

The discussion is divided into two subsections. First, the relationship between the distortions produced in the face milling experiments and the measured machining-

induced residual stresses is described. In the second subsection, the study is extended to a more complex part geometry (employing the validated FEM model) to understand the influence of machining-induced residual stresses on part distortion and to obtain transferrable knowledge.

5.1. Effect of machining-induced residual stresses in flat specimens

The finishing condition A generated higher maximum vertical displacements than finishing condition B, as can be seen in Fig. 9. The effect of machining-induced residual stresses on the final distortion could be calculated as the difference between the final distortion ($u_{z\text{final}}$) and the distortion caused by the initial residual stresses ($u_{z\text{IRS}}$): $\Delta u_{z\text{MRS}}=u_{z\text{final}}-u_{z\text{IRS}}$. The finishing condition A produced a maximum distortion of $\Delta u_{z\text{MRS}} = 0.68$ mm at the centre of the part, 45% higher than the one produced by finishing condition B ($\Delta u_{z\text{MRS}} = 0.47$ mm).

Fig. 10 shows a scheme with the main variables involved in the distortions caused by machining-induced residual stresses in simple geometries. It could be extended to surface residual stresses, such as those generated by shot peening. It should be clarified that the drawing is not scaled. The surface layer i affected by the machining process has a residual stress profile $\sigma_{\text{RS}xi}$ perpendicular to the cross section of the layer. We can define a local axis n_i perpendicular to the machined surface, where the origin of the axis n_i is at the surface, as can be seen in Fig. 10. The resultant force of the residual stress profile can be calculated using (eq. 1), where $\text{d}A_i$ is a differential area of the cross section of the surface layer. If the surface layer has a width b_i, the resultant force can be calculated by (eq. 2).The location of the resultant force with respect to local axis system is given by (eq. 3). Using (eq.3) and taking into account the geometry of the part, the

position of the resultant force in the global coordinate system is defined by z_i. The position of the centroidal axis of the part is given by z_c. As can be seen in the scheme, the resultant force of the machining-induced residual stresses causes on the right side of the transverse section a bending moment M_{yi}, that can be calculated employing (eq. 4). As a result, the part is bent in the opposite direction to balance the disequilibrium caused by M_{yi}. Note that M_{yi} considers the magnitude and sign of residual stresses and their position, a general expression.

$$R_{xi} = \int \sigma_{\mathrm{RS}xi} \cdot \mathrm{d}A_i \qquad \text{(eq.1)}$$

$$R_{xi} = \int \sigma_{\mathrm{RS}xi} \cdot b_i \mathrm{d}_{ni} \qquad \text{(eq.2)}$$

$$n_{ci} = \frac{\int \sigma_{\mathrm{RS}xi} \cdot n_i \mathrm{d}_{Ai}}{\int \sigma_{\mathrm{RS}xi} \cdot \mathrm{d}_{Ai}} \qquad \text{(eq.3)}$$

$$M_{yi} = R_{xi} \cdot (z_i - z_c) \qquad \text{(eq.4)}$$

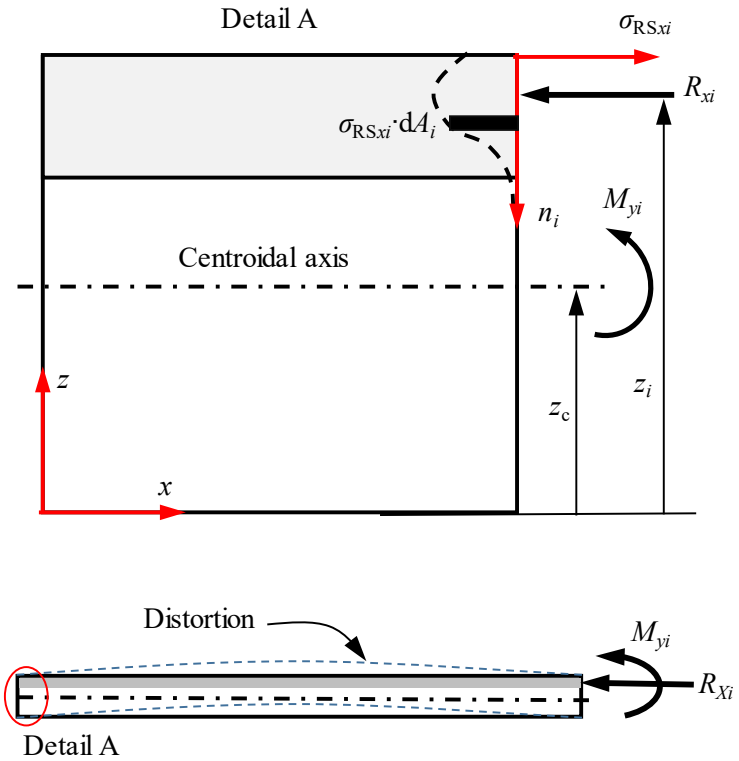

Fig. 10. Scheme of the main variables involved in the distortions caused by surface residual stresses

In this study the bending moment generated by finishing condition A was M_{yA} = -53.78 N·mm and the finishing condition B produced M_{yB} = -37.04 N·mm. Therefore, the bending moment caused by finishing condition A was 45% higher than the one generated by B, and as explained before, led to a distortion Δu_{zMRS} 45% higher. In addition, both finishing condition generated a negative bending moment M_y on the right side of the part, and consequently the distorted part showed a concave shape to reach the static equilibrium.

5.2. Effect of machining-induced residual stresses in complex geometries

The procedure described in the preceding section allows understanding the effect of machining-induced residual stresses on the distortions of flat specimens. Nevertheless, airframe structures, such as ribs, possess more complex geometries, usually formed with many ribs and webs. Indeed, the effect of residual stresses induced in the flanges or in the webs on the distortions of an aeroframe may differ considerably.

To obtain more general understanding about the effect of machining-induced residual stresses on distortions of real aerostructures an additional study was carried out using the FEM model validated in this research. For that purpose, we selected an inverted T shape part geometry which contains the main features of a typical aerostructure (flanges and webs). The geometry of the part can be seen in Fig. 11. The inverted T was 100 mm wide, 38 mm high and 400 mm long. It had a 6 mm thick rib along the centre line of the part, and the thickness of the web was of 6 mm as well.

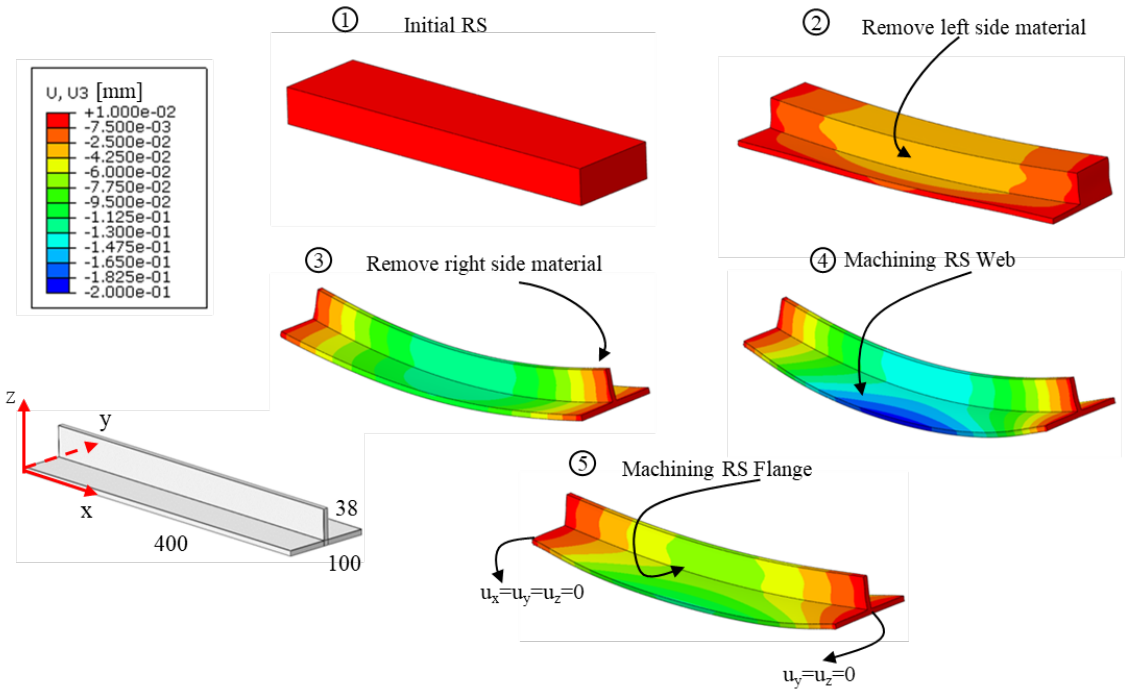

Fig. 11. Geometry and simulation process of the inverted T shaped part. Example of combination 1

Fig. 11 shows the simulation process of this additional study. The simulation was divided into four steps: 1) introduction of initial residual stresses, 2) removal of the left side material cut during the machining, 3) removal of the right side material cut during the machining, 4) introduction of the machining-induced residual stresses in the web and finally 5) assignation of the residual stresses generated by machining in the flange. It should be clarified that the residual stresses induced by the machining process in the web and flange could be introduced in a unique step. However, we decided to introduce in two different steps because in doing so, it is possible to quantify separately the effect of the residual stresses generated in the web and flange on the distortions of the part. The material selected was the aluminium 7175-T7351, the aluminium used in the experiments. The part was meshed using C3D8R type elements with a global nodal distance of 1 mm, and the mesh was refined in the surface layer affected by the cutting process to add the machining-induced stresses in the web and flange respectively. The

following boundary conditions were defined: the displacements of the left edge were restricted (u_x=u_y=u_z=0), and also the vertical and lateral displacements of the right edge (u_y=u_z=0). To analyse the effect of different cutting conditions a total of 9 combinations of machining conditions were simulated as summarised in Table 3.

It should be noted that in this new study we have added a third finishing condition identified as finishing C, which was tested on a part of 7175-T7351 aluminium with different geometry compared to Type I specimens. The same tool and inserts were used to machine this at cutting speed of 550 m/min, depth of cut off 0.25 mm, feed rate the same as in finishing A and B. Fig. 12 shows the residual stress profile of finishing C.

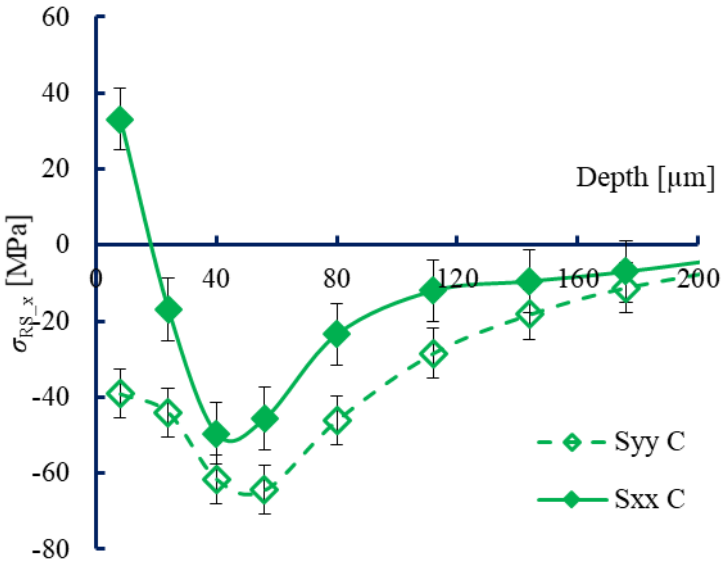

Fig. 12. Machining Residual Stress for Finishing C

Table 3. Combination of machining conditions and residual stresses used in the study of the inverted T part

Combination	RS of the web	RS of the flange
1	Finishing A	Finishing A
2	Finishing B	Finishing A
3	Finishing C	Finishing A
4	Finishing A	Finishing B
5	Finishing B	Finishing B
6	Finishing C	Finishing B
7	Finishing A	Finishing C
8	Finishing B	Finishing C
9	Finishing C	Finishing C

Fig. 11 shows the distortions (*z* displacements) generated in each step of the simulation for the combination 1. The material removal (step 2 and 3) generated a convex deformation shape of the part (the difference between the initial *z* position and *z* position after removing material was $\Delta u_{z1\text{-}3}<0$). In the fourth step, the residual stresses generated by machining were added in the surface layer of the web. Again, these machining-induced residual stresses led to a slightly more negative vertical displacement (the difference between the *z* position after the second step and *z* position once machining induced RS were introduced in the web was $\Delta u_{z3\text{-}4}<0$) in the *x* direction as well as a concave deformation shape in the *y* direction (due to the *y* direction of the machining-induced residual stress). However, the introduction of the machining-induced residual stresses in the web reduced considerably the distortion of the part, although it was still convex ($\Delta u_{z4\text{-}5}>0$) in the x direction and concave in the *y* direction.

The same trend was observed in the nine simulated cases. Therefore, these results confirm that the effect of machining-induced residual stresses generated in the webs and flanges contributes in a different manner (magnitude and sign) to the final distortion of the part.

Fig. 13 compares the maximum vertical displacement (z axis) of the 9 combinations analysed in this additional study, only taking into account the distortions along x direction. The maximum distortion after each step of the simulation is shown to evaluate the effect of initial residual stresses, machining-induced residual stresses in the web and flange respectively. As explained in the preceding paragraph, the introduction of machining-induced residual stresses in the surface of the web did not affect very much the distortion of the part, they increased the maximum distortion around 12% when using finishing condition A, 7% with condition B and 11.7% with condition C. Nevertheless, the effect of the residual stresses induced by machining in the flange was more significant: reducing by 59% using the finishing condition A, 36% with finishing condition B and 55 % with finishing condition C. As a result of the sum of all the effects, the combination 2 obtained the highest distortion (-0.097 mm) and combination 4 the lowest (-0.061 mm). Therefore, this highlights the possibility to reduce the distortion of parts by controlling machining-induced residual stresses.

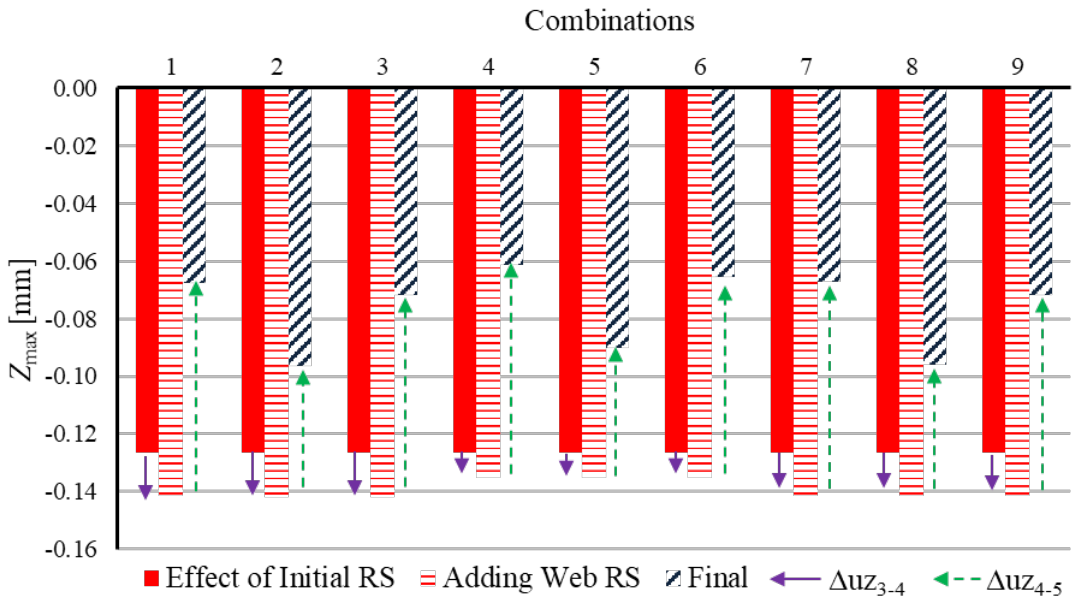

Fig. 13. Maximum vertical displacement (z_{max}) of the part for the 9 analysed combinations after each step of the simulation process.

The effect of machining-induced residual stresses on the distortions of a flat part can be explained using (eq. 1), (eq. 2), (eq. 3) and (eq. 4) respectively. The same approach can be used to describe the results of a more complex geometry if we apply those equations to each surface affected by the machining process. The total distortion caused by the machining-induced residual stresses will be proportional to the total bending moment M_{ytot} , as indicated in (eq. 5).

$$M_{ytot} = \sum M_{yi} \qquad \text{(eq.5)}$$

A scheme of the effect of machining-induced residual stresses on the distortions induced in the inverted T part can be seen in Fig. 14. In this case, the centroidal axis was above the web. Therefore, the compressive residual stresses introduced in the surface of the web led to convex distortions, but the compressive residual stresses in the surface of the flange generated distortions in the opposite direction which reduced the distortion generated by

the initial residual stresses. For the same cutting condition the force resultant of the web $R_{x\text{web}}$ was greater than the force resultant of the flange $R_{x\text{flange}}$, because the affected surface was wider. Nevertheless, the effect of distortions of the machining-induced residual stresses in the flange was significantly higher than the influence of the residual stresses introduced in the surface of the web. This occurs because the distance from the position of the force resultant to the centroidal axis of the part is much higher in the flange, and therefore the bending moment $M_{y\text{flange}}$ is much higher than $M_{y\text{web}}$.

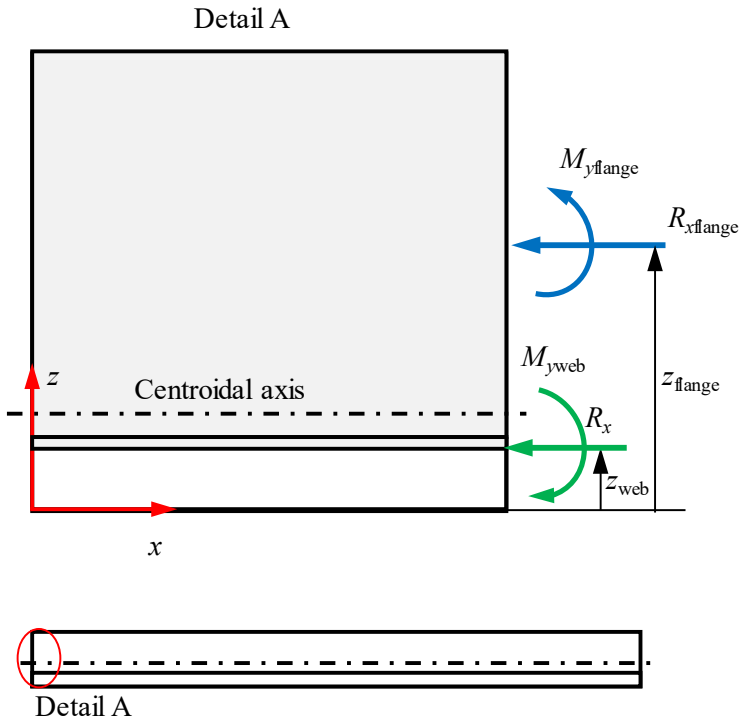

Fig. 14. Scheme showing the effect of the residual stresses induced in the web and flange on the distortions of the inverted T part

Using the approach described in the preceding paragraph and shown in the Fig. 14, it is possible to calculate the relationship between the bending moment caused by machining-

induced residual stresses and distortions. Fig. 15 shows the maximum vertical displacement generated by the bending moment related to the machining-induced residual stresses introduced in the web, flange and the sum of both (combination). As it can be seen in the graph, there is a linear relationship between the bending moment and the maximum distortion. Therefore, the bending moment, which is linked to the magnitude, sing and location of machining-induced residual stresses, can be used to quantify the distortions.

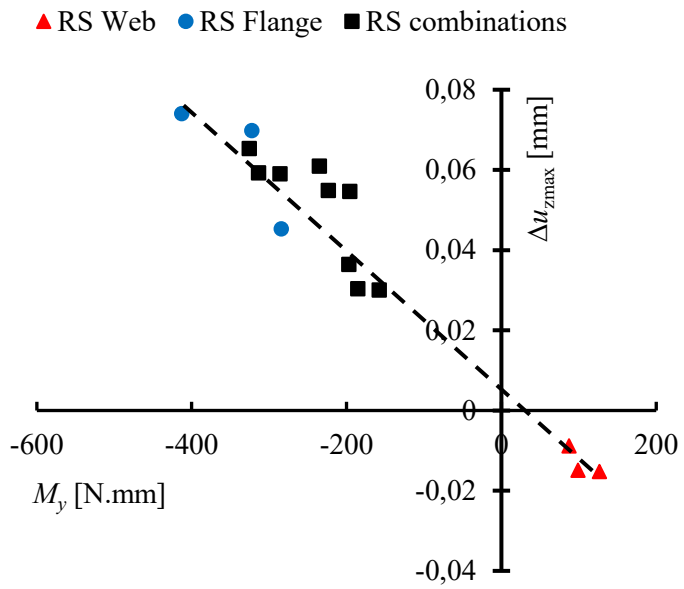

Fig. 15. Maximum vertical displacement produced by the bending moment related to machining-induced residual stresses.

6. Conclusions

The influence of machining-induced residual stresses on the distortions of large aluminium parts used in aerostructures was analysed in this work. The main conclusions are:

(1) This work demonstrates that final distortion of large aluminium parts is sensitive to machining-induced residual stresses. The influence of machining-induced residual stresses on the final distortion depends on the sign (tensile or compressive), magnitude and position of the residual stress profiles generated by the cutting process with respect to the neutral plane of the part. Interestingly, This effect can be estimated by the equivalent bending moment caused by the distribution of residual stresses of each machined surface.

(2) Both initial residual stresses of the original workpiece and residual stresses generated by the cutting process affect the final distortion of thin-walled large aluminium parts. The FEM model that includes initial residual stresses and machining-induced residual stresses predicts the final distortion accurately, in this work with an inaccuracy lower than 15%.

(3) The FEM model allows determining the machining conditions that minimise part distortions. In this work, employing this procedure a reduction of 40% was achieved in an inverted T shape aluminium part.

Acknowledgments

The authors thank the Basque and Spanish Governments for the financial support given to the projects HDAUTO (EC_2016_1_0015) and TEMPROCEN (CIEN_IDI-20141299).

The authors would like to thank Naieli Zabala for writing assistance.

References

1. Sim WM (2009) Residual stress engineering in manufacture of aerospace structural parts. *Filton, UK: Airbus SAS.*, www.transport-research.info Accessed 20 September 2017
2. Li JG, Wang SQ (2016). Int. J. Adv. Manuf. Technol. 89 (1-4), 997-1012. doi: 10.1007/s00170-016-9066-6
3. Masoudi S, Amini S, Saeidi E, Eslami-Chalander H. (2015). Effect of machining-induced residual stress on the distortion of thin-walled parts. Int. J. Adv. Manuf. Technol. 76(1-4), 597-608. doi: 10.1007/s00170-014-6281-x
4. Brinksmeier E, Sölter J (2009) Prediction of shape deviations in machining. CIRP Annals-Manuf. Technol. 58(1), 507-510. doi: 10.1016/j.cirp.2009.03.123
5. Denkena B, Dreier S (2014) Simulation of Residual Stress Related Part Distortion. In: Denkena, B. (Ed.), Proceedings of the 4th Machining Innovations Conference, Hannover, Germany, pp. 105-113
6. Cerutti X, Mocellin K (2015) Influence of the machining sequence on the residual stress redistribution and machining quality: analysis and improvement using numerical simulations. Int J Adv Manuf Technol. doi: 10.1007s00170-015-7521-4
7. Denkena B, De León-García L, Köhler J (2006) Influence of high performance cutting operations on the residual stresses of aluminum structural work-pieces. In: Grant, I. (Eds.), Proceedings of ICAS 2006, 25th International Congress of the Aeronautical Sciences, Hamburg, Germany

8. Tang ZT, Yu T, Xu LQ, Liu ZQ (2013) Machining deformation prediction for frame components considering multifactor coupling effects. Int. J. Adv. Manuf. Technol. 68(1-4), 187-196. doi: 10.1007/s00170-012-4718-7
9. Li B, Jiang X, Yang J, Liang SY (2015) Effects of depth of cut on the redistribution of residual stress and distortion during the milling of thin-walled part. J. Mater. Process. Technol. 216, 223-233. doi: 10.1016/j.jmatprotec.2014.09.016
10. Yang Y, Li M, Li KR (2014) Comparison and analysis of main effect elements of machining distortion for aluminum alloy and titanium alloy aircraft monolithic component. Int. J. Adv. Manuf. Technol. 70(9-12), 1803-1811. doi: 10.1007/s00170-013-5431-x
11. Huang X, Sun J, Li J (2015) Finite element simulation and experimental investigation on the residual stress-related monolithic component deformation. Int. J. Adv. Manuf. Technol. 77(5-8), 1035-1041. DOI 10.1007/s00170-014-6533-9
12. Prime MB (2000) Cross-sectional Mapping of Residual Stresses by Measuring the Surface Contour After a Cut. J. Eng. Mater. Technol 123(2), 162-168. DOI:10.1115/1.1345526
13. Grant PV, Lord JD, Whitehead PS, Fry TA (2005) The application of fine increment hole drilling for measuring machining-induced residual stresses. Appl. Mech. Mater. 3-4, 105-110. DOI: 10.4028/www.scientific.net/AMM.3-4.105
14. Jayanti, S., Ren, D., Erickson, E., Usui, S., Marusich, T., Marusich, K., and Elanvogan, H., (2013) Predictive modeling for tool deflection and part distortion

of large machined components. Procedia CIRP 12, 37-42. DOI 10.1016/j.procir.2013.09.008

15. BI, Y.B., Cheng, Q.L., Dong, H.Y., Ke, Y.L. (2009) Machining distortion prediction of aerospace monolithic components. J Zhejiang Univ-sc A 10(5):661–668. DOI:10.1631/jzus.A0820392
16. Wan, M., Ye, X.Y., Zhang, W.H. (2017) Theoretical prediction of machining-induced residual stresses in three-dimensional oblique milling processes. Int. J. Mech. Sci. 133:426-437. DOI:10.1016/j.ijmecsci.2017.09.005
17. Berruti ,T., Lavella, M., Gola, M.M. (2009) Residual Stresses on Inconel 718 Turbine Shaft after turning. Mach Sci Technol 13(4):543–560. Doi:10.1080/10910340903451472